

Two-Way Quantum Time Transfer: A Method for Daytime Space-Earth Links

Randy Lafler,¹ Mark L. Eickhoff,² Scott C. Newey,² Yamil Nieves Gonzalez,² Kurt E. Stoltenberg,² J. Frank Camacho,³ Mark A. Harris,³ Denis W. Oesch,³ and R. Nicholas Lanning¹

¹*Air Force Research Laboratory, Directed Energy Directorate, Kirtland AFB, NM, United States**

²*The Boeing Company, Albuquerque NM, United States*

³*Leidos, Albuquerque NM, United States*

(Dated: July 17, 2023)

Remote clock synchronization is crucial for many classical and quantum network applications. Current state-of-the-art remote clock synchronization techniques achieve femtosecond-scale clock stability utilizing frequency combs, which are supplementary to quantum-networking hardware. Demonstrating an alternative, we synchronize two remote clocks across our freespace testbed using a method called two-way quantum time transfer (QTT). In one second we reach picosecond-scale timing precision under very lossy and noisy channel conditions representative of daytime space-Earth links with commercial off-the-shelf quantum-photon sources and detection equipment. This work demonstrates how QTT is potentially relevant for daytime space-Earth quantum networking and/or providing high-precision secure timing in GPS-denied environments.

Precise synchronization of remote clocks is important for position, navigation, and timing (PNT), high speed transactions, distributed computing, quantum networking, and many other applications. A common technique used to synchronize remote clocks is based on global positioning system (GPS) public signals, which can achieve nanosecond-scale synchronization [1]. If more precision is desired, or one is operating in a GPS-denied environment, other techniques must be used. Optical two-way time and frequency transfer (O-TWTFT) utilizes frequency combs to synchronize two remote clocks to femtosecond precision [2, 3]. To date, demonstrations of O-TWTFT have been performed between stationary sites [2–4] and slow moving drones, < 25 m/s. However, femtosecond-scale synchronization may be excessive for many applications. As an alternative, the White Rabbit (WR) protocol can achieve picosecond-level precision and has been investigated for quantum-networking synchronization [5–7]. It was designed for wireline fiber-optic applications, but has been implemented wirelessly [8] and considered for space applications [9]. Perhaps the most straightforward optical-time-transfer technique uses pulsed lasers, photodetectors, and software-based correlation methods. For example, time transfer by laser link (T2L2) demonstrations have achieved picosecond-scale precision between remote ground stations operating in common view with the Jason-2 satellite after a 1000-s acquisition [10]. However, these techniques utilize systems and hardware nonessential to quantum communication.

Another technique consists of utilizing the femtosecond-scale temporal correlations of photon pairs created in spontaneous-parametric-down conversion (SPDC) photon sources. In this case, the relative time offset between two remote clocks is measured with

the following procedure: (1) a series of photon pairs are separated and transmitted to two remote sites, (2) the photons are detected and their arrival times are time-tagged based on the respective local clock, (3) after sufficient detection events are collected, the series of arrival times from each site are combined and correlation methods are used to find the clock offset. This technique was first proposed in Ref. [11] and we refer to it as quantum time transfer (QTT). One-way QTT enables relative clock synchronization [12], and two-way QTT enables absolute clock synchronization [13]. Subsequently, we investigated the suitability of this method for lossy and noisy channel conditions commensurate with daytime Earth-satellite quantum downlinks [14].

In this letter, we report remote clock synchronization and ranging with two-way QTT during conditions representative of bi-directional Earth-satellite links. Our system achieves picosecond-scale timing precision during these challenging conditions with commercial off-the-shelf (COTS) hardware. We discuss the measured clock offset, the overlapping Allan deviation, the time deviation, the propagation distance between the transmitter sites, and the coincidence-to-accidental ratio (CAR) of the quantum correlation signals relative to the measured atmospheric conditions.

Our freespace quantum-communication testbed is located at the Starfire Optical Range (SOR), Kirtland AFB, NM in the Southwestern United States. The transceiver sites are the same sites utilized in Ref. [15], but are enhanced for two-way propagation using the arrangement in Fig. 1. We tune the Alice-to-Bob direction to be representative of a low-Earth orbit (LEO) downlink; we set the beam divergence to impose the correct geometric loss, we use a white light source to scatter noise photons into the channel, we use a heat source to add scintillation, and we utilize a closed-loop adaptive-optics (AO) system to monitor and compensate for atmospheric turbulence [15].

In the Bob-to-Alice “uplink” direction, the quantum

* AFRL.RDSS.OrgMailbox@us.af.mil

DISTRIBUTION A: Approved for public release; distribution is unlimited.

Public Affairs release approval AFRL-2023-3154

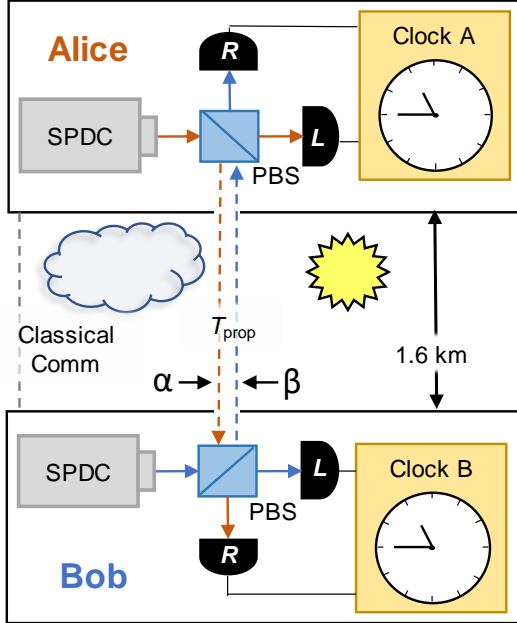


FIG. 1: Schematic of two-way QTT field experiment. Each site is equipped with an SPDC bi-photon source, local L and receive R detectors, and an independent local clock consisting of a time tagger, a rubidium frequency standard, and a PC. The sites are separated by a 1.6 km freespace channel with propagation time T_{prop} . The Alice-to-Bob and Bob-to-Alice propagation directions are denoted by α and β , respectively. The classical channel is utilized for sharing time tags.

signal is precompensated by the AO system, and photons arrive at Alice with similar efficiency to the downlink direction. However, for Earth-satellite uplinks, the quantum signal is transmitted at a point-ahead angle such that it intercepts the LEO satellite. As a consequence, the quantum signal travels a slightly different path than the downlink beacon that drives the AO system. This typically results in more loss due to reduced compensation of atmospheric-turbulence effects caused by isoplanatism [16]. Therefore, to make our “uplink” direction more realistic, we apply an additional 2 dB attenuation in software to the true coincidences in the receive channel at the Alice site. This level of attenuation corresponds to AO compensation with an ideal beacon in the point-ahead direction. This could be achieved using a boom or a small beacon satellite leading the quantum satellite. Closing the AO loop on a *downlink* beacon would result in ~ 10 dB more attenuation. Applying this level of attenuation we observe temporary loss of synchronization due to the relatively low-performance sources in this field experiment. A higher pair rate and heralding efficiency source at the ground station would increase the attenuation tolerance and relax the requirement for the beacon in the point-ahead direction [14].

Figure 1 gives a schematic of the two-way QTT components. The sites labeled Alice and Bob each have a

Thor Labs SPDC810 bi-photon source and a pair of Exelitas SPCM-AQRH detectors labeled L and R for local and received, respectively. The clock system is comprised of a Picoquant Hydralarp 400 time tagger, a Stanford Research Systems PRS10 Rubidium frequency standard (RbFS), and a PC. Alice and Bob create a pair of photons, detect one of the pair with their local detector L , and send the other photon across the 1.6 km freespace channel to the other site where it is detected with a receive detector R . The detection times t in the Alice-to-Bob direction α are related by

$$t_{A,L} = t_{B,R} - T_{\text{prop}} - \delta, \quad (1)$$

where the subscripts A and B correspond to the local clocks at Alice and Bob, respectively, T_{prop} is the propagation time, and δ is the absolute clock offset. Similarly, the detection times in the Bob-to-Alice, β , direction are

$$t_{A,R} = t_{B,L} + T_{\text{prop}} - \delta. \quad (2)$$

One-way QTT is performed independently in both the α and β directions, and the resulting relative clock offsets τ_α and τ_β are

$$\begin{aligned} \tau_\alpha &= t_{A,L} - t_{B,R} = -T_{\text{prop}} - \delta \\ \tau_\beta &= t_{B,L} - t_{A,R} = -T_{\text{prop}} + \delta. \end{aligned} \quad (3)$$

Combining Eq. 3 we find the absolute clock offset and the propagation time [13]

$$\begin{aligned} \delta &= \frac{\tau_\beta - \tau_\alpha}{2} \\ T_{\text{prop}} &= -\frac{\tau_\beta + \tau_\alpha}{2}. \end{aligned} \quad (4)$$

In Fig. 2(a) we show the measured turbulence parameters $[r_0, \sigma_f^2]$ over which we performed two-way QTT, where each data point represents the average during a one second acquisition. The projections onto the Hufnagel Valley $1 \times$, $2 \times$, and $3 \times HV_{5/7}$ theoretical turbulence profiles [15] show that the atmospheric conditions were similar or worse than an Earth-satellite downlink. We select two continuous 1-hr acquisitions that are representative of daytime (blue) and nighttime (black) atmospheric conditions in order to highlight the performance of the two-way QTT algorithm under each condition. All other data is shown in gray. In Fig. 2(b) we show the CAR of the QTT correlation signal in the α direction as a function of the background sky radiance H_b during the daytime scenario, where larger CAR corresponds to greater confidence that the QTT algorithm correctly identified the true correlation signal. As expected, Fig. 2(b) shows that the CAR increases as the background sky radiance H_b decreases. Furthermore, it shows the robustness of the QTT algorithm to high background levels, that is, the QTT algorithm reliably finds the true correlation signal even as the CAR approaches 1.

Next, we consider the timing performance of our two-way QTT clock system. We do this by utilizing the following two logical or “software” clocks. One is drifting,

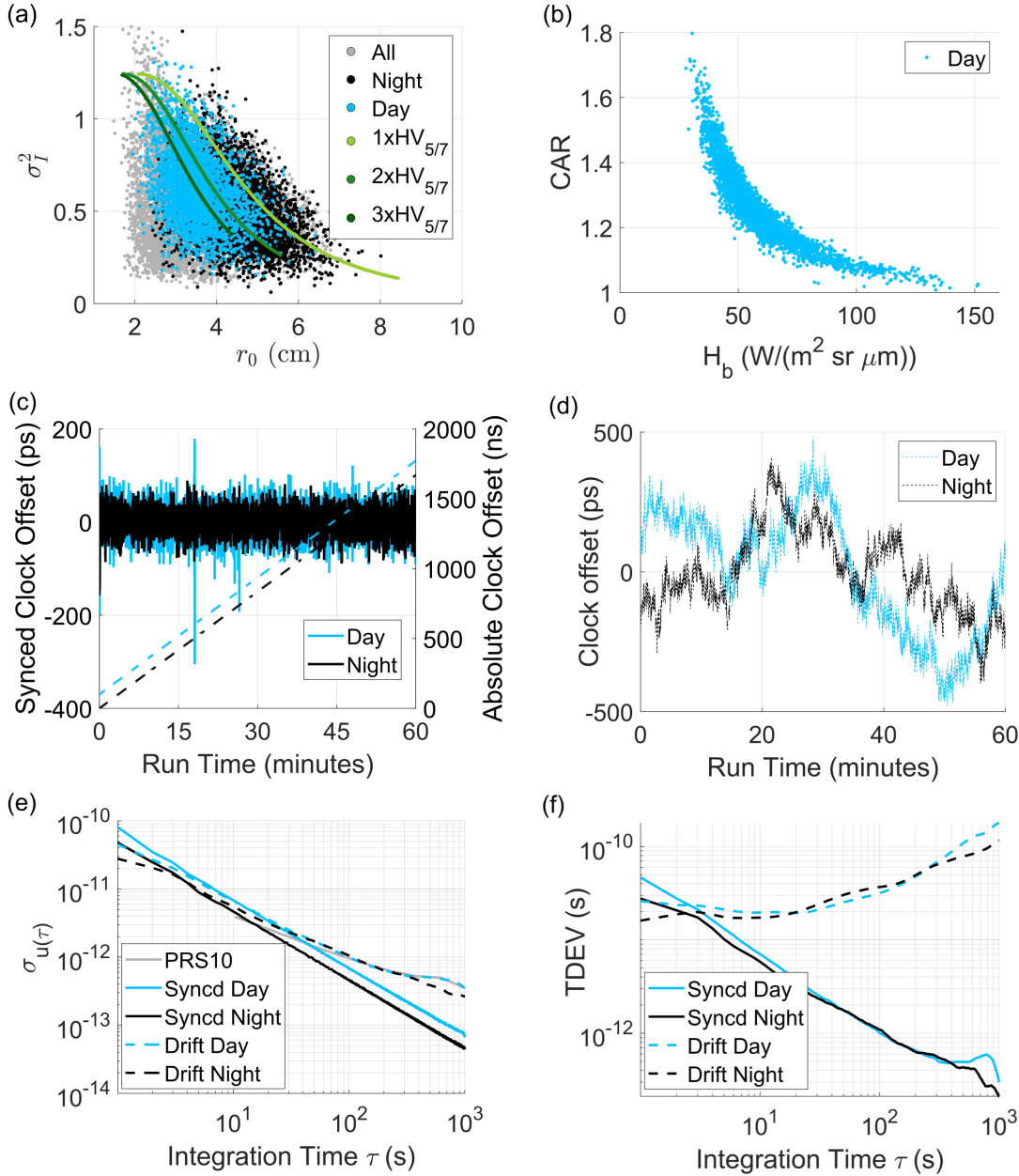


FIG. 2: (a) The measured turbulence parameters $[r_0, \sigma_I^2]$ and their projections onto the $1\times$, $2\times$, and $3\times HV_{5/7}$ theoretical turbulence profile [15]. The representative 1-hr acquisitions under daytime and nighttime conditions are in blue and black, respectively. All other data is shown in gray. (b) The CAR as a function of the background sky radiance H_b for the daytime scenario. The (c) absolute offset of the synchronized clock (solid curves and left axis) and the drifting clock (dashed curves and right axis). In (d) we take the drifting clock offset measurements and remove the linear trend to highlight the fluctuations in picoseconds. In (e) and (f) we plot the overlapping Allan deviation and time deviation measured by the synchronized (solid) and drifting (dashed) clocks, respectively. The gray line is the Allan deviation quoted in the PRS10 RbFS operators manual.

that is, the local hardware clocks drift apart and the absolute clock offset δ is simply tracked. The other is synchronized, that is, we perform the following recursive synchronization algorithm. First, we estimate the current clock drift ΔU based on prior measurements or estimates. Next, we predict how far the clocks will drift

before the next measurement by adding $\Delta U \times T_a$ to the most recent offset measurement, where our acquisition time $T_a = 1$ s. We move the synchronized clock ahead based on the prediction, and thus the next measurement is the difference from the prediction. The result is shown in Fig. 2(c) for the daytime and nighttime scenarios with

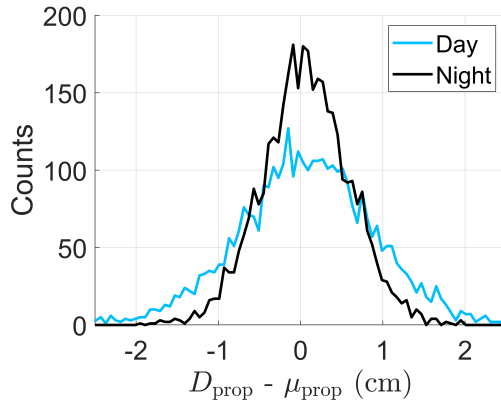


FIG. 3: Histogram of the difference between the propagation distance D_{prop} and the mean propagation distance μ_{prop} for the daytime (blue) and nighttime (black) scenarios.

the synchronized (solid curves and left axis) and drifting (dashed curves and right axis) clocks. The standard deviations are 27.1 and 39.7 ps for the nighttime and daytime scenarios, respectively. As expected, the timing jitter is smaller at night. Meanwhile, the drifting clock shows that the local clocks drift from each other at a rate of ~ 340 ps per second on average. Figure 2(d) shows the absolute clock offset δ according to the drifting clock after the mean clock drift is removed. Furthermore, we see that the two-way QTT algorithm can run continuously without losing synchronization for an extended period of time under challenging channel conditions.

The Allan deviation is a standard method to characterize the stability and noise profile of a clock system [18]. In Fig. 2(e) we show the overlapping Allan deviation, where the solid and dashed curves are the synchronized and drifting clocks, and the daytime and nighttime scenarios are blue and black, respectively. The gray curve is the Allan deviation reported in the user manual of the Stanford Research Systems PRS10 RbFS. The slopes for the drifting and synchronized clocks are approximately

-0.6 and -1 , respectively. Furthermore, we measure the time deviation (TDEV) [18], which has a slope of $-1/2$ according to the synchronized clock. Combined these results indicate that the predominate noise is white FM and white PM for the drifting and synchronized clocks, respectively. Visually, one can see these different noise profiles in Figure 2(c) and (d).

Assuming a constant speed of light c , one can use Eq. 4 to find the propagation distance. In Fig. 3 we plot the propagation-distance distribution for the nighttime and daytime 1-hour acquisitions with the average propagation distance subtracted. We find that the mean of both distributions is $\mu_{\text{prop}} = 1.644403$ km with standard deviations σ_{prop} 1.04 cm and 0.57 cm for the daytime and nighttime scenario, respectively. The width of the daytime distribution is larger than the nighttime distribution because the timing jitter is worse during the daytime scenario.

In this letter we report a remote clock synchronization and ranging demonstration over daytime space-Earth channel conditions utilizing a protocol we call two-way quantum time transfer. Our algorithm synchronizes to 10's of ps after only 1 second of integration with COTS hardware. Furthermore, we precisely measured the propagation distance of our testbed to a precision better than 1 cm. We analyze the performance of the protocol using the Allan and time deviations with synchronized and drifting software clocks.

The authors acknowledge program management support from Valerie Knight, Ryan Riley, Ian Blake, and Adrian Lewis AFRL. The views expressed are those of the author and do not necessarily reflect the official policy or position of the Department of the Air Force, the Department of Defense, or the U.S. government. The appearance of external hyperlinks does not constitute endorsement by the U.S. Department of Defense (DoD) of the linked websites, or the information, products, or services contained therein. The DoD does not exercise any editorial, security, or other control over the information you may find at these locations.

Approved for public release; distribution is unlimited. Public Affairs release approval AFRL-2023-3154

[1] M. A. Lombardi, L. M. Nelson, A. N. Novick, and V. S. Zhang, Cal Lab: International Journal of Metrology **8**, 26 (2001).

[2] F. R. Giorgetta, W. C. Swann, L. C. Sinclair, E. Baumann, I. Coddington, and N. R. Newbury, Nature Photonics **7**, 434 (2013).

[3] L. C. Sinclair, W. C. Swann, H. Bergeron, E. Baumann, M. Cermak, I. Coddington, J.-D. Deschênes, F. R. Giorgetta, J. C. Juarez, I. Khader, et al., Applied physics letters **109**, 151104 (2016).

[4] E. D. Caldwell, J.-D. Deschenes, J. Ellis, W. C. Swann, B. K. Stuhl, H. Bergeron, N. R. Newbury, and L. C. Sinclair, Nature **618**, 721 (2023).

[5] T. Gerrits, I. Burenkov, Y.-S. Li-Baboud, A. Rahmouni, D. Anand, O. Slattery, A. Battou, S. Polyakov, et al., in *CLEO: QELS_Fundamental Science* (Optica Publishing Group, 2022), pp. FM1C-2.

[6] M. Alshowkan, P. G. Evans, B. P. Williams, N. S. Rao, C. E. Marvinney, Y.-Y. Pai, B. J. Lawrie, N. A. Peters, and J. M. Lukens, in *CLEO: QELS_Fundamental Science* (Optica Publishing Group, 2022), pp. FM1C-4.

[7] K. Schatz, B. Amies-King, S. Albosh, R. Kumar, and M. Lucamarini, in *Quantum Technology: Driving Commercialisation of an Enabling Science III* (SPIE, 2023), vol. 12335, pp. 104–109.

[8] J. E. Gilligan, E. M. Konitzer, E. Siman-Tov, J. W. Zobel, and E. J. Adles, IEEE transactions on ultrasonics, ferroelectrics, and frequency control **67**, 1946 (2020).

[9] M. Jamrozy, M. Gumiński, G. Kasprowicz, R. Romaniuk, and K. Poźniak, in *Photonics Applications in Astronomy, Communications, Industry, and High-Energy Physics Experiments 2015* (SPIE, 2015), vol. 9662, pp. 357–362.

[10] P. Exertier, E. Samain, N. Martin, C. Courde, M. Laas-Bourez, C. Foussard, and P. Guillemot, *Advances in Space Research* **54**, 2371 (2014).

[11] A. Valencia, G. Scarcelli, and Y. Shih, *Applied Physics Letters* **85**, 2655 (2004).

[12] C. Ho, A. Lamas-Linares, and C. Kurtsiefer, *New Journal of Physics* **11**, 045011 (2009).

[13] J. Lee, L. Shen, A. Cerè, J. Troupé, A. Lamas-Linares, and C. Kurtsiefer, *Applied Physics Letters* **114**, 101102 (2019).

[14] R. Lafler and R. N. Lanning, arXiv preprint arXiv:2211.00737 (2022).

[15] M. T. Gruneisen, M. L. Eickhoff, S. C. Newey, K. E. Stoltenberg, J. F. Morris, M. Bareian, M. A. Harris, D. W. Oesch, M. D. Oliker, M. B. Flanagan, et al., *Physical Review Applied* **16**, 014067 (2021).

[16] R. K. Tyson, *Principles of adaptive optics* (CRC press, 2015).

[17] R. N. Lanning, M. A. Harris, D. W. Oesch, M. D. Oliker, and M. T. Gruneisen, *Phys. Rev. Applied* **16**, 044027 (2021), URL <https://link.aps.org/doi/10.1103/PhysRevApplied.16.044027>.

[18] W. J. Riley and D. A. Howe, *Handbook of frequency stability analysis* (US Department of Commerce, National Institute of Standards and Technology, 2008).